Heavy quark photoproduction in the $k_\perp$-factorization approach

C. Brenner Mariotto,* M. B. Gay Ducati,† and M. V. T. Machado‡
Instituto de Física, Universidade Federal do Rio Grande do Sul, Caixa Postal 15051, 91501-970 Porto Alegre, RS, Brazil
(Received 19 August 2002; published 27 December 2002)

We investigate heavy quark photoproduction based on the $k_\perp$-factorization approach, focusing on the results from the saturation model. The deviations between the results using the unintegrated gluon distribution considering the saturation model and the derivative of the collinear gluon distribution are analyzed. Total cross sections and p_T distributions are analyzed in detail, giving the deviations between the results of the color dipole approximation and the complete semihard approach.

DOI: 10.1103/PhysRevD.66.114013 PACS number(s): 13.60.Hb, 12.38.Bx, 14.65.Dw, 14.65.Fy

I. INTRODUCTION

The investigation of heavy quark production at high energies provides a better understanding of the hadron internal structure. In particular, the heavy quark masses are large enough to be taken as a hard scale, making the strong coupling constant small and allowing a perturbative QCD treatment of the process. Heavy quarks are produced in the clean $\gamma p \to Q\overline{Q}$ reaction at the DESY ep collider HERA, where the incident photon (real or virtual) probes the proton target at a high center of mass energy W. There is a large amount of data on heavy flavor production at HERA, which have been a boom to studies analyzing the interface between hard and soft regimes [1,2]. However, the data for open heavy quark production are limited by small statistics and the intermediate energy interval between the fixed target experiments and the high energy at HERA have not been covered yet. In hadroproduction at the Fermilab Tevatron $p\overline{p}$ collider, the situation is slightly better, giving precise measurements of the transverse momentum distribution of the heavy quarks produced [3,4].

The underlying mechanism for heavy quark production at HERA is photon-gluon fusion: a photon coupled to the scattered electron interacts with a gluon from the proton by producing a quark-antiquark pair, e.g., $c\overline{c}$ (charm) or $b\overline{b}$ (bottom). In the collinear QCD approach, based on the well known collinear factorization theorem [5], the process is described through the convolution of on-shell matrix elements, encoding the partonic subprocesses, with the parton distribution functions. At high energies, the gluon is the parton which drives the dynamics, evolving through the virtualities obeying the Dokshitzer-Gribov-Lipatov-Altarelli-Parisi (DGLAP) evolution equations [6]. The transverse momenta of the incident particles are taken as zero and in the computation of the cross sections one averages over two transverse polarizations of the initial gluon. A computation of the process requires the knowledge of the gluon momentum distribution in the proton and the calculation of the γg subprocess. The gluon density as a function of the longitudinal momentum fraction x and virtuality scale Q^2 is known to an accuracy of a few percent from a global analysis of scaling violations of the proton structure function F_2 measured at HERA [7–9]. The QCD matrix elements of the partonic process have been calculated in next-to-leading order (NLO) accuracy [10]. Still substantial theoretical uncertainties come from the heavy quark mass and from the renormalization and factorization scales μ_R and μ_F.

The collinear factorization approach has produced a successful description of single-particle distributions and total cross sections for heavy quark production. On the other hand, despite many phenomenological successes, results within this approach are in contradiction with data on azimuthal correlations and on distributions in the transverse momentum of the heavy quark pair produced [11] (for quarkonium production see, e.g., Refs. [2,12]). This problem is in general cured by introducing an intrinsic transverse momentum distribution (intrinsic $k_\perp$) for the incident partons, parametrized using a Gaussian profile. However, the mean value of intrinsic $k_\perp$ needed to describe azimuthal correlations and the p_T spectrum can be as high as $\langle k_\perp \rangle \simeq 1$ GeV or even 2–3 GeV, which is not suitable from nonperturbative arguments. Moreover, recent calculations using known NLO results [13] for bottom hadroproduction in the collinear approach undershoot Tevatron data [14] by a factor of 2 or 3, suggesting that an important contribution to the computed observables is missing.

At high energies another factorization theorem emerges, the $k_\perp$-factorization or semihard approach [15–17]. The relevant diagrams are considered with the virtualities and polarizations of the initial partons, taking into account the transverse momenta $q_{1\perp}$ and $q_{2\perp}$ of the incident partons. The processes are described through the convolution of off-shell matrix elements with the unintegrated parton distribution $\mathcal{F}(x,k_\perp)$. The latter can recover the usual parton distributions in the double-logarithmic limit (DLL) by its integration over the transverse momentum $k_\perp$. In the asymptotic energy limit, the unintegrated gluon distribution should obey the Balitskiĭ-Fadin-Kuraev-Lipatov (BFKL) evolution equation [18]. At the present, there is a lack of an accurate determination of this quantity at the same level as the usual parton densities. The matrix elements computed for the relevant subprocesses within the $k_\perp$-factorization approach are already more involved than those needed in the collinear approach at the LO level. On the other hand, a significant part

*Electronic address: mariotto@if.ufrgs.br
†Electronic address: gay@if.ufrgs.br
‡Electronic address: magnus@if.ufrgs.br

of the NLO and some of the NNLO corrections to the LO contributions in the collinear approach, related to the contribution of nonzero transverse momenta of the incident partons, are already included in the LO contribution within the $\boldsymbol{k}_\perp$-factorization formalism [11]. Moreover, part of the virtual corrections can be resummed in the unintegrated gluon function [11]. Recently, the computation of NLO corrections to the subprocesses has been completed and full calculations at this level should appear in the near future [19]. An important feature of the approach is the equivalence at leading logarithmic approximation with the color dipole picture [20], which has been used in much phenomenology at HERA [21]. In addition, a very important issue is the consistency of the $\boldsymbol{k}_\perp$-factorization approach including nonleading-log effects with collinear factorization beyond leading order [22]: the coefficient functions and the splitting functions providing $q(x,Q^2)$ and $G(x,Q^2)$ are supplemented with the all-order resummation of the $\alpha_s \ln(1/x)$ contributions at high energies, in contrast with a calculation in fixed order perturbation theory.

Two additional ingredients should be taken into account when considering the semihard approach: the infrared sector and saturation effects. The unintegrated gluon function should evolve in tranverse momentum through the BFKL evolution at high energies, leading to the diffusion in $\boldsymbol{k}_\perp$ of the initial gluons in the evolution process [23]. In this diffusion scenario the transverse momenta values are spread out into the infrared (and ultraviolet) region, where the perturbative description is not completely reliable. Therefore, the evolution should take properly into account the correct behavior in that region. The recently calculated nonlinear corrections to the BFKL approach [24] introduce a natural treatment for these difficulties, where the saturation scale Q_s provides a suitable cutoff controlling the infrared problems. As the longitudinal momentum fraction $x \simeq Q^2/W^2$ decreases, unitarity corrections become important and control the steep growth of the gluon distribution. In this domain the gluon distribution can saturate completely or acquire a mild logarithmic increase. The most appealing approach taking into account both the notions of infrared behavior (confinement) and parton saturation phenomenon is the saturation model [25], which is an eikonal-type model based on the color dipole picture of high energy interactions. In this approach the physical picture is considerably simplified and the expression for the saturation scale is promptly calculated. The adjustable parameters of the model are obtained from a fit to small-x HERA data of the inclusive structure function and the photoproduction total cross section, and are suitable for further applications to more exclusive quantities such as open heavy quark production.

This paper is organized as follows. In the next section we present the main formulas for heavy quark photoproduction within the $\boldsymbol{k}_\perp$-factorization approach, defining the relevant kinematical variables. Furthermore, we investigate the unintegrated gluon distribution from the saturation model in comparison with the results from the derivative of the integrated gluon distribution, $x\mathcal{G}(x,\boldsymbol{k}_\perp)$. In Sec. III, we present our results for the total cross section for charm and bottom photoproduction, as well as estimates for the $p_\perp$ distribution of the heavy quark pair produced. We investigate in detail the deviations in the results when one confronts the dipole approximation and a conservative $\boldsymbol{k}_\perp$-factorization procedure; namely, the choice of scale for the coupling constant and the suitable longitudinal momentum fraction entering in the unintegrated gluon function. The predictions from the derivative of the collinear gluon function are also studied. In the last section, we present the conclusions and final considerations.

II. HEAVY QUARK PHOTOPRODUCTION IN THE $k_\perp$ FACTORIZATION

In this section we investigate the quasireal photon scattering off a proton in the semihard approach. In light quark photoproduction there is poor knowledge concerning the effective light quark mass, which is associated with nonperturbative aspects of the process. This problem is naturally solved in heavy quark photoproduction, because of the heavy quark mass. The semihard approach is valid in the domain where the following double inequality holds: $s \gg \mu^2 \simeq \hat{s} \gg \Lambda^2_{QCD}$, i.e., the typical parton interaction scale μ^2 is much higher than the QCD cutoff parameter Λ^2_{QCD}, and much lower than the center of mass energy $\sqrt{s}$. The $\boldsymbol{k}_\perp$-factorization approach can resum in the leading logarithmic approximation all the contributions proportional to $[\alpha_s \ln(\mu^2/\Lambda^2_{QCD})]^n$, $[\alpha_s \ln(\mu^2/\Lambda^2_{QCD})\ln(1/x)]^n$, and $[\alpha_s \ln(1/x)]^n$, where the first one corresponds to the collinear DGLAP resummation [6], the second one to the double-logarithmic contribution, and the last one to the BFKL resummation [18]. Such resummation leads to the unintegrated gluon distribution $\mathcal{F}(x,\boldsymbol{k}_\perp)$, which can also depend on the scale μ^2. It gives the probability of finding a parton carrying a longitudinal momentum fraction x and transverse momentum $\boldsymbol{k}_\perp$. Requiring that in the DLL limit the transverse photoabsortion total cross section written in the $\boldsymbol{k}_\perp$-factorization approach be consistent with the same limit from the DGLAP approach, the collinear gluon distribution is given by the unintegrated one in the following way:

$$xG(x,\mu^2) = \int^{\mu^2} \frac{dk_\perp^2}{k_\perp^2} \mathcal{F}(x,k_\perp^2), \tag{1}$$

where μ^2 is the scale of the process, which can be Q^2, the heavy quark mass, or the $p_\perp$ of the particles produced, for instance. In particular, in obtaining Eq. (1), a strong ordering condition $\boldsymbol{k}_\perp^2 \ll \boldsymbol{p}_\perp^2 \ll \mu^2$ is considered, where $\boldsymbol{p}_\perp$ is the transverse momentum of the quark-antiquark loop in the photon vertex.

In order to compute the cross section of a physical process [26,27], the unintegrated gluon function should be convoluted with the off-shell matrix elements for the relevant partonic subprocesses. In these matrix elements the polarization tensor of the virtual gluon is given by $L^{(g)}_{\mu\nu} = \overline{\varepsilon_g^\mu \varepsilon_g^{*\nu}} = k_\perp^\mu k_\perp^\nu / |\boldsymbol{k}_\perp|^2$. In the following we will calculate the total and differential cross sections of heavy quark photoproduction (charm and bottom) taking into account the diagrams

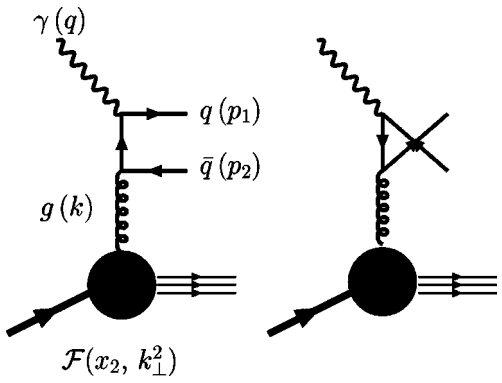

FIG. 1. The leading order QCD diagrams for heavy-quark production via photon-gluon fusion. The momenta of the particles are shown and the blob represents the gluon emission chain encoded in the unintegrated gluon distribution $\mathcal{F}(x_2,\boldsymbol{k}_\perp^2)$.

shown in Fig. 1. For convenience, one can define the Sudakov variables for the process $ep\to Q\overline{Q}X$ at high energies,

$$p_1=\alpha_1 P_1+\beta_1 P_2+\boldsymbol{p}_{1\perp}, \quad q=x_1 P_1+\boldsymbol{q}_\perp, \tag{2}$$

$$p_2=\alpha_2 P_1+\beta_2 P_2+\boldsymbol{p}_{2\perp}, \quad k=x_2 P_2+\boldsymbol{k}_\perp, \tag{3}$$

where, as shown in Fig. 1, p_1 and p_2 are the four-momenta of the produced heavy quarks, and q and k are the photon and the gluon four-momenta, respectively. The corresponding transverse momenta are $\boldsymbol{p}_{1\perp}$, $\boldsymbol{p}_{2\perp}$, $\boldsymbol{q}_\perp$, and $\boldsymbol{k}_\perp$. The electron and proton momenta are denoted by P_1 and P_2. In the center of mass frame of the process, one has $P_1=(\sqrt{s}/2,0,0,\sqrt{s}/2)$, $P_2(\sqrt{s}/2,0,0,-\sqrt{s}/2)$, $P_1^2=P_2^2=0$, and $(P_1\cdot P_2)=s/2$, with $\sqrt{s}$ being the center of mass energy. From simple inspection of Eqs. (2) and (3) and using the energy-momentum conservation law, one obtains the relations

$$p_1^2=p_2^2=m_Q^2, \quad q^2=\boldsymbol{q}_\perp^2, \quad k^2=\boldsymbol{k}_\perp^2, \tag{4}$$

$$\boldsymbol{q}_\perp+\boldsymbol{k}_\perp=\boldsymbol{p}_{1\perp}+\boldsymbol{p}_{2\perp}. \tag{5}$$

The Sudakov variables can be written in terms of the transverse masses $m_{1,2\perp}^2=m_Q^2+\boldsymbol{p}_{1,2\perp}^2$, where m_Q is the heavy quark mass, and the heavy quark rapidities $y_{1,2}^*$, in the following way:

$$\alpha_1=\frac{m_{1\perp}}{\sqrt{s}}\exp(y_1^*), \quad \alpha_2=\frac{m_{2\perp}}{\sqrt{s}}\exp(y_2^*), \tag{6}$$

$$\beta_1=\frac{m_{1\perp}}{\sqrt{s}}\exp(-y_1^*), \quad \beta_2=\frac{m_{2\perp}}{\sqrt{s}}\exp(-y_2^*), \tag{7}$$

$$x_1=\alpha_1+\alpha_2, \quad x_2=\beta_1+\beta_2, \tag{8}$$

where in the photoproduction case $q=P_1$, the variable x_1 simplifies to $x_1=1$ and one can define $\alpha_1\equiv z$ and $\alpha_2\equiv 1-z$. The z and $(1-z)$ variables correspond to the longitudinal momentum fraction carried by the heavy quark having transverse momenta $\boldsymbol{p}_{1\perp}$ and $\boldsymbol{p}_{2\perp}$, respectively.

Having introduced the relevant definitions and variables, the differential cross section for the photoproduction process is expressed as the convolution of the unintegrated gluon function with the off-shell matrix elements [15,26,28],

$$\frac{d\sigma(\gamma p\to Q\overline{Q}X)}{d^2\boldsymbol{p}_{1\perp}}=\int dy_1^* d^2\boldsymbol{k}_\perp \frac{\mathcal{F}(x_2,\boldsymbol{k}^2)|\mathcal{M}|^2(\text{off shell})}{\pi\alpha_2}, \tag{9}$$

where the off-shell LO matrix elements are given by [28,26]

$$|\mathcal{M}|^2(\text{off shell}) = \alpha_{em}\alpha_s(\mu^2)e_Q^2\left[\frac{z^2+(1-z)^2}{[(p_2-k)^2-m_Q^2][(p_1-k)^2-m_Q^2]} + \frac{2m_Q^2}{k_\perp^2}\left(\frac{z}{(p_1-k)^2-m_Q^2}-\frac{1-z}{(p_2-k)^2-m_Q^2}\right)^2\right], \tag{10}$$

where $\alpha_{e.m.}=1/137$ is the electromagnetic coupling constant and e_Q is the electric charge of the heavy quark produced. The scale μ in the strong coupling constant will be specified later on. In general, it is taken to be equal to the gluon virtuality, $\mu^2=\boldsymbol{k}^2$, in close connection with the Brodsky-Lepage-Mackenzie (BLM) scheme [29]. In the leading $\ln(1/x)$ approximation, α_s should take a constant value. When the transverse momenta of the incident partons are sufficiently smaller than those of the produced heavy quarks, the result from the collinear approach is recovered. The final expression for the photoproduction total cross section considering the direct component of the photon can be written as [27]

$$\sigma_{tot}^{phot}=\frac{\alpha_{e.m.}e_Q^2}{\pi}\int dz d^2\boldsymbol{p}_{1\perp} d^2\boldsymbol{k}_\perp \frac{\alpha_s(\mu^2)\mathcal{F}(x_2,\boldsymbol{k}_\perp^2;\mu^2)}{\boldsymbol{k}_\perp^4} \times\left\{[z^2+(1-z)^2]\left(\frac{\boldsymbol{p}_{1\perp}}{D_1}+\frac{(\boldsymbol{k}_\perp-\boldsymbol{p}_{1\perp})}{D_2}\right)^2 + m_Q^2\left(\frac{1}{D_1}+\frac{1}{D_2}\right)^2\right\}, \tag{11}$$

where $D_1\equiv\boldsymbol{p}_{1\perp}^2+m_Q^2$ and $D_2\equiv(\boldsymbol{k}_\perp-\boldsymbol{p}_{1\perp})^2+m_Q^2$.

In Eq. (11) the unintegrated gluon function was allowed to depend also on the scale μ^2, since some parametrizations take this scale into account in the computation of that quantity (see, for instance Ref. [30] for a compilation of a number of them). We are now ready to calculate the total and differential cross sections for the process, provided a suitable input for the function $\mathcal{F}(x_2,\boldsymbol{k}_\perp^2;\mu^2)$. The practical procedure in this paper is to consider one of the simplest parametrizations available, covering a consistent treatment of the infrared region and taking into account the expected saturation effects at high energies. These features are fullfilled in the saturation model, which it is briefly reviewed in the following and it will be conveniently contrasted with the results coming from the derivative of the collinear gluon function,

$$x\mathcal{G}(x,\boldsymbol{k}_\perp^2)=\frac{\partial[xG(x,\boldsymbol{k}_\perp^2)]}{\partial\ln\boldsymbol{k}_\perp^2}, \tag{12}$$

where $G(x,\mu^2)$ is the integrated gluon distribution, which can be taken from the available parametrizations in the literature [7–9].

A. The saturation model

The saturation model [25] is based on the color dipole picture of the interaction, represented in the target rest frame where the transverse size $\boldsymbol{r}$ of the dipole quark-antiquark coming from the virtual photon Fock state fluctuations is fixed during the interaction. This representation can be recovered from the $\boldsymbol{k}_\perp$-factorization approach in the leading-logarithmic approximation through the Fourier transform between the transverse size and the transverse momentum spaces. The photoabsortion total cross section is written as a convolution of the virtual photon wave function with the effective cross section for the interaction dipole target,

$$\sigma_{tot}^{\gamma^* p}(x,Q^2)=\int dz\int d^2\boldsymbol{r}[|\Psi_T(z,\boldsymbol{r},Q^2)|^2+|\Psi_L(z,\boldsymbol{r},Q^2)|^2]\sigma_{dip}(x,\boldsymbol{r}), \tag{13}$$

where the dipole cross section interpolates between the color transparency behavior for small size dipole configuration and the confinement features for large dipole sizes. It reads

$$\sigma_{dip}=\sigma_0\left[1-\exp\left(-\frac{\boldsymbol{r}^2}{4R_0^2(x)}\right)\right], \tag{14}$$

$$R_0^2(x)=\frac{1}{\mathrm{GeV}^2}\left(\frac{x}{x_0}\right)^{\lambda}, \tag{15}$$

where $R_0(x)$ is the saturation radius which decreases when $x\to 0$. The parameters σ_0, x_0, and λ are determined from a fit to small-x HERA data. An additional parameter is the effective light quark mass $m_q=140$ MeV, which is needed to produce finite results for the photoproduction total cross section. The saturation scale is defined as $Q_s^2=1/R_0^2(x)$: when $rQ_s/2\ll 1$ the model reproduces color transparency, $\sigma_{dip}\sim r^2$, whereas when $rQ_s/2\geqslant 1$ the cross section tends to a constant at large rQ_s (it simulates confinement), $\sigma_{dip}\sim\sigma_0$. In the region $rQ_s/2\sim 1$, the model simulates the physics from the multiple scattering resummation of gluon exchanges in an eikonal-type way representing the black disk limit of the proton. In the original model, the coupling constant is considered fixed as $\alpha_s=0.2$ and in order to consider the formal limit of photoproduction, the Bjorken variable has been modified in the following way:

$$x=x_{Bj}\left(1+\frac{4m_q^2}{Q^2}\right)=\frac{Q^2+4m_q^2}{W^2}. \tag{16}$$

Starting from the $\boldsymbol{k}_\perp$-factorization approach for the total photoabsortion cross section, but disregarding the transverse momentum dependence in the argument of the strong coupling constant and in the variable x, an analytical result for the Fourier transform between the spaces can be obtained,

$$\sigma_{dip}(x,\boldsymbol{r})=\frac{2\pi}{3}\int\frac{d^2\boldsymbol{k}_\perp}{\boldsymbol{k}_\perp^4}\alpha_s\mathcal{F}(x,\boldsymbol{k}_\perp^2)(1-e^{i\boldsymbol{k}_\perp\cdot\boldsymbol{r}})(1-e^{-i\boldsymbol{k}_\perp\cdot\boldsymbol{r}}). \tag{17}$$

Therefore, Eq. (17) can be used to extract the unintegrated gluon function from the model in $\boldsymbol{r}$ space, once the dipole cross section has a finite limit at $\boldsymbol{r}\to\boldsymbol{0}$, denoted as $\sigma_{dip}^{(\infty)}(x)$. It can be written as [31]

$$\alpha_s\mathcal{F}(x,\boldsymbol{k}_\perp^2)=\frac{3}{4\pi}\int\frac{d^2\boldsymbol{r}}{(2\pi)^2}\exp(i\boldsymbol{k}_\perp\cdot\boldsymbol{r})\times[\sigma_{dip}^{(\infty)}(x)-\sigma_{dip}(x,\boldsymbol{r})]\boldsymbol{k}_\perp^4 \tag{18}$$

$$=\frac{3}{8\pi^2}\int_0^\infty dr\,r J_0(k_\perp r)[\sigma_{dip}^{(\infty)}(x)-\sigma_{dip}(x,r)]k_\perp^4\,. \tag{19}$$

After writing down the expression for the unintegrated gluon function to be employed in the studies of the next section, some considerations are in order. The saturation model is a quite successful approach for the small-x region and it was also extended to simultaneously describe diffractive deep inelastic scattering. However, when $x\to 1$, the approach is no longer suitable and threshold correction factors should be introduced. The simplest way to implement this is to consider dimensional-cutting rules: for a subprocess having n_{spec} spectator quarks which do not interact with the photon, the corresponding threshold factor is given by $(1-x)^{2n_{spec}-1}$. For example, including light and charm quarks, the number of spectators is $n_{spec}=4$ and in our analysis we include the multiplicative correction factor $(1-x)^7$ in the unintegrated gluon function from the saturation model. In the next section, such a correction provides a correct description of the fixed target energy region, whereas the results from the original model remain unaltered at intermediate and high energies.

For our purposes in this investigation, we use the following parameters corresponding to the parametrization which includes the charm quark: $\sigma_0=29.12$ mb, $\lambda=0.277$, and $x_0=4.1\times 10^{-3}$ [25]. From Eqs. (18) and (14), the unintegrated gluon distribution from the original saturation model supplemented by the threshold factor is given by

$$\mathcal{F}(x,\boldsymbol{k}_\perp^2)=\frac{3\sigma_0}{4\pi^2\alpha_s}R_0^2(x)\boldsymbol{k}_\perp^4\exp[-R_0^2(x)\boldsymbol{k}_\perp^2](1-x)^7. \tag{20}$$

We illustrate in Fig. 2, shown in the plot on the left, the unintegrated gluon function from Eq. (20) as a function of the transverse momentum $\boldsymbol{k}_\perp^2$ at typical values of the x variable, covering large and small longitudinal momentum fractions. We remark that the small-x region corresponds to $x\leqslant 10^{-2}$. Its main features are quite clear: the function is peaked at $\boldsymbol{k}_\perp^2=2Q_s^2$, with a narrow distribution around this

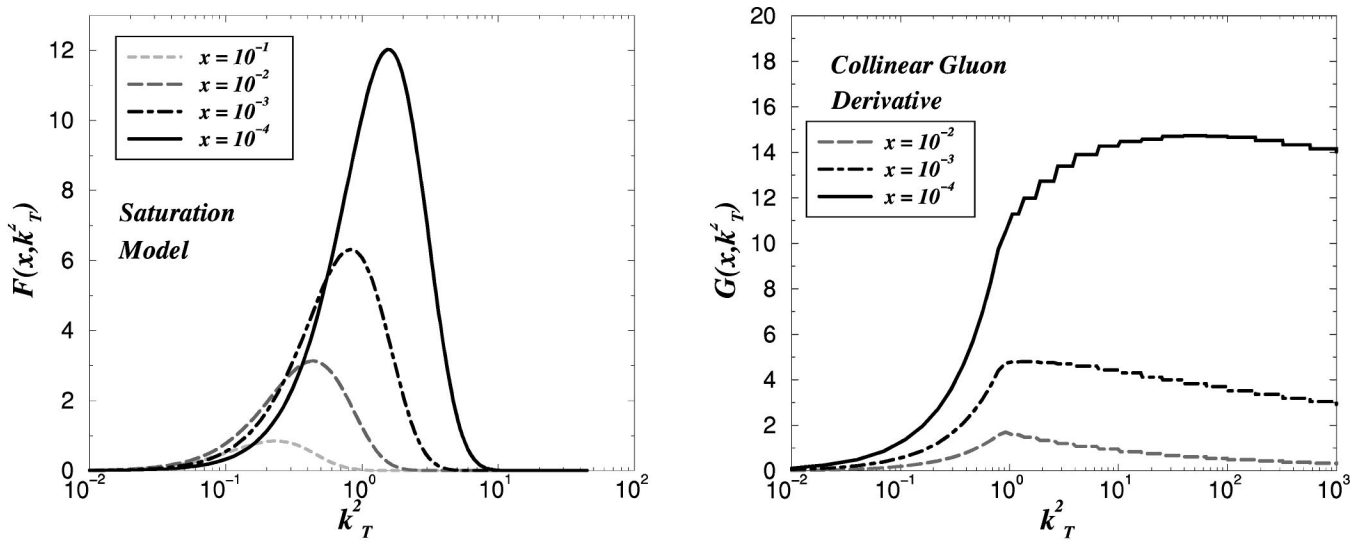

FIG. 2. Left plot: The unintegrated gluon distribution from the saturation model as a function of $\boldsymbol{k}_\perp^2$ for typical x values. Right plot: The derivative of the collinear gluon distribution (LO GRV98 parametrization) as a function of $\boldsymbol{k}_\perp^2$ for typical x values.

value, being slightly asymmetric for large x. Therefore, the peak is shifted to larger $\boldsymbol{k}_\perp^2$ as x decreases. The most important feature is a large contribution from the very small transverse momentum sector $\boldsymbol{k}_\perp \leqslant 1$ GeV^2 at large x. Moreover, the unintegrated gluon distribution is strongly suppressed for large $\boldsymbol{k}_\perp^2$ due to the missing parton evolution in the original model. This shortcoming is cured in the recent implementation of the DGLAP evolution for the unintegrated gluon distribution [31].

In order to investigate the importance of a $\boldsymbol{k}_\perp$ enhancement coming from a QCD parton cascade emission, we present in the plot on the right in Fig. 2 the result from the derivative of the collinear gluon distribution $\mathcal{G}(x,\boldsymbol{k}_\perp^2)$, where the LO Glück-Reya-Vogt 1998 (GRV98) [9] gluon parametrization was chosen for the calculation. The use of this quantity gives the possibility of checking the consistency of introducing elements from DGLAP evolution in the $\boldsymbol{k}_\perp$-factorization approach. That parametrization has the virtuality $Q_0^2 = 0.8$ GeV^2 as the initial evolution scale and below this value one should make an assumption about the behavior of $\mathcal{G}$. In our analysis we apply the following procedure:

$$\mathcal{G}(x,\boldsymbol{k}_\perp^2) = \boldsymbol{k}_\perp^2 \left.\frac{\partial[xG(x,\boldsymbol{k}_\perp^2)]}{\partial \boldsymbol{k}_\perp^2}\right|_{\boldsymbol{k}_\perp^2 = Q_0^2} \Theta(Q_0^2 - \boldsymbol{k}_\perp^2) + \frac{\partial[xG(x,\boldsymbol{k}_\perp^2)]}{\partial \ln \boldsymbol{k}_\perp^2}\Theta(\boldsymbol{k}_\perp^2 - Q_0^2), \tag{21}$$

where the first term can recover $xG(x,Q_0^2)$ by integration over transverse momentum from 0 up to Q_0^2. However, we emphasize that such a procedure is not unique and other *Ansätze* can be introduced. For instance, we can consider a lower integration limit $\boldsymbol{k}_{\perp min}^2 \simeq Q_0^2$, emphasizing that in the theoretical curves the cutoff mainly would affect the overall magnitude of the cross section. As expected, in our results the transverse momentum spectrum is broader, in contrast with the saturation model. In the small-x region the deviation is huge both in behavior and in overall normalization. The large-x region is correctly described since the collinear gluon function is adjusted on the whole kinematical range at HERA. It has been verified that by using the NLO collinear gluon distribution the deviations are negligible [32]. A technical remark is the pronged behavior of $\mathcal{G}(x,\boldsymbol{k}_\perp^2)$ above Q_0^2, which has no physical meaning, since it has to do with the grid interpolation routines used to obtain the collinear gluon function, and this effect is smoothed out in the integrated quantities and should not affect our later results.

In the next section we investigate the saturation model in the computation of the total and differential heavy quark photoproduction cross sections, and a comparison with the derivative of the collinear gluon function will be used in order to study the effects of QCD evolution.

III. RESULTS AND DISCUSSION

The available data [33–36] on heavy quark (charm and bottom) photoproduction range from energies W of fixed target experiments about tens of GeV, up to the high energy HERA data around $W \sim 200$ GeV. Kinematically, the low energy data correspond to $x \simeq 10^{-1}$ and the high energy ones to $x \simeq 10^{-4}$. The experimental errors are rather large and the intermediate region between low and high energies is not covered by measurements. Beauty production at HERA is suppressed by two orders of magnitude with respect to charm, due to the larger mass and smaller electric charge of the b quark.

The total and differential cross sections are computed from Eq. (11) and the unintegrated gluon function from the saturation model, Eq. (20). The heavy quark mass was considered as $m_c = 1.5$ GeV for charm and $m_b = 4.8$ GeV for bottom. In order to investigate in detail the results emerging from the $\boldsymbol{k}_\perp$-factorization approach and in an attempt to go beyond the leading logarithmic $\ln(1/x)$ approximation, we

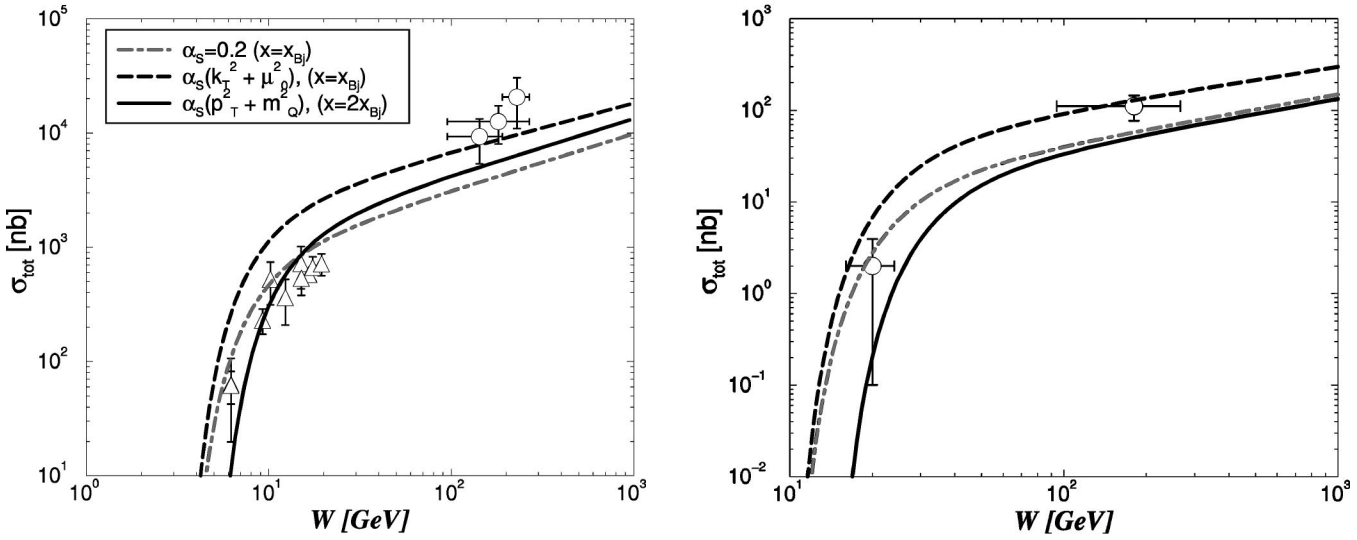

FIG. 3. Left plot: The charm photoproduction total cross section as a function of center of mass energy W and the $\boldsymbol{k}_\perp$-factorization approach results using the saturation model and different technical procedures in the calculation (see text). Right plot: The bottom photoproduction total cross section as a function of center of mass energy W and the $\boldsymbol{k}_\perp$-factorization approach results using the saturation model and different technical procedures in the calculation (see text).

have considered in our analysis the following procedures.

(1) We keep the original features of the saturation model, namely, a fixed strong coupling constant $\alpha_s=0.2$ and the longitudinal momentum fraction x_2, which is the photoproduction limit of the Bjorken x_{Bj}, given by Eq. (16), entering in the unintegrated gluon distribution. This procedure is equivalent to using the color dipole picture and the saturation model, as performed in the detailed study of Ref. [37]. The result is shown in the dot-dashed curves in Fig. 3, for charm (plot on the left) and bottom (plot on the right) total cross sections. There is good agreement with the low energy data, whereas the high energy data are underestimated. The good description of the fixed target data is ensured by the threshold correction factor $(1-x)^7$, since the original model would already overestimate the data at intermediate energies. At high energies, those threshold effects are completely negligible at $W\gtrsim 20$ GeV for charm and $W\gtrsim 50$ GeV for bottom. Similar conclusions are obtained in Ref. [37]. One small difference between the procedure above and the calculations in Ref. [37] is the prescription for the longitudinal momentum fraction being $x_Q=m_Q^2/z(1-z)$ in the latter. If we consider a mean value $z=0.5$ for the quark momentum fraction, the results are completely equivalent. The very close similarity between our predictions and those of Ref. [37] corroborates our procedure of calculation.

(2) We allow the argument of the strong coupling constant to run with the scale $\mu^2=\boldsymbol{k}_\perp^2+\mu_0^2$. This procedure is still very close to the saturation model, and it is the general procedure used in calculating observables by other groups [26,27]. The term μ_0^2 is introduced in order to avoid divergences coming from the coupling constant in the infrared region. The value $\mu_0^2=1$ GeV^2 has been used, motivated by the value of the saturation scale Q_s, ensuring that the low transverse momentum region is dominated by that scale. The result seems to spoil the previous good agreement at low energies, as shown in the dashed curves in Fig. 3. However, the high energy data are described in better agreement than in the previous procedure. In conclusion, the introduction of a running coupling in the calculation shifts the overall normalization toward higher values at high energies, by enhancing the $\boldsymbol{k}_\perp^2$ profile in the unintegrated cross section.

(3) As a final aspect, we consider a conservative procedure concerning the $\boldsymbol{k}_\perp$-factorization approach. The argument of the strong coupling constant is let to run with the scale $\mu^2=\boldsymbol{p}_\perp^2+m_Q^2$, where $\boldsymbol{p}_\perp$ is the transverse momentum of the heavy quark produced. Moreover, we have a different prescription for the x_2 variable from that in Eq. (16). The correct value for the longitudinal momentum fraction entering in $\mathcal{F}(x_2,\boldsymbol{k}_\perp^2)$ is given by the definitions in Eqs. (8) and (7); namely, the momentum fraction is given by

$$x_2=\frac{m_{1\perp}^2}{zW^2}+\frac{m_{2\perp}^2}{(1-z)W^2}=\frac{m_Q^2+(\boldsymbol{p}_\perp-\boldsymbol{k}_\perp)^2}{z}+\frac{m_Q^2+\boldsymbol{p}_\perp^2}{1-z}, \tag{22}$$

where one has made use of the relations in Eqs. (6) and (7) and the energy-momentum conservation law, Eq. (5). Although Eq. (22) is well defined, it is involved for practical computations and for simplicity we rely on the following approximation. We benefit from the results of the $\boldsymbol{k}_\perp$-factorization approach applied to ep collisions, in particular for the proton structure function, performed in Ref. [38]. There, it was verified that for not too high virtualities Q^2 (including photoproduction) a suitable approximation is $x_2=2x_{Bj}$. This value is obtained from a careful investigation of the contributions in the transverse momentum integration range for the corresponding DGLAP piece and for the semihard approach. The results using the procedure above are

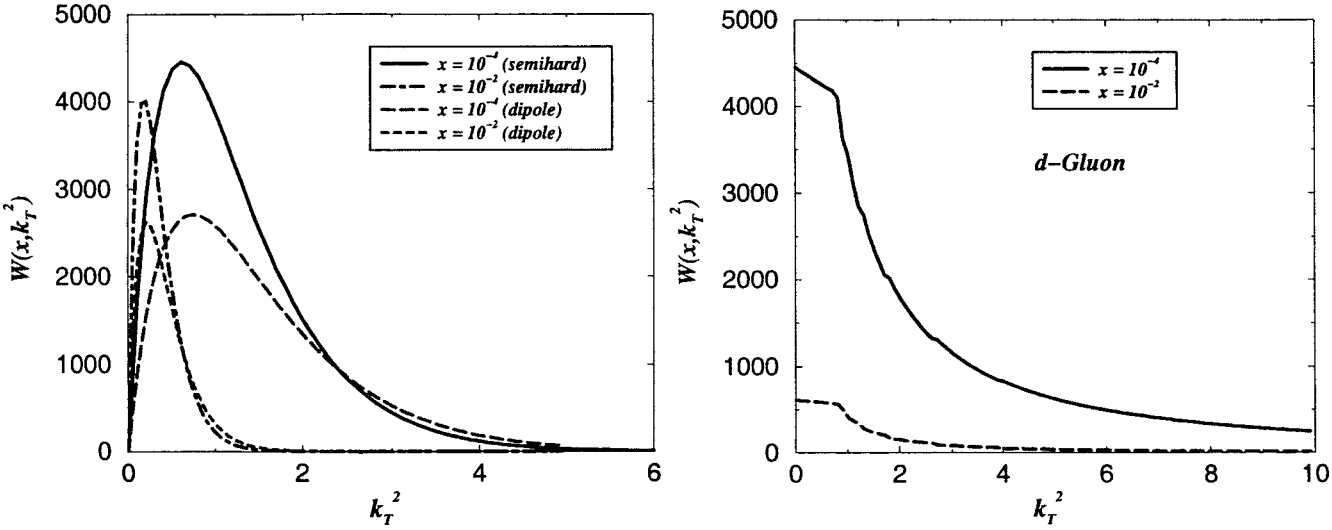

FIG. 4. Left plot: The $k_\perp$ profile (charm) for the unintegrated cross section from the saturation model for two different procedures concerning the coupling constant and momentum fraction scale (see text). Right plot: The $k_\perp$ profile (charm) for the unintegrated cross section from the derivative of the collinear gluon distribution (LO GRV98 parametrization).

shown as the solid lines in Fig. 3, presenting an intermediate behavior between the first and the second procedures. In particular, the fixed target data are described in good agreement and the results for high energy data are slightly improved compared to the equivalent dipole result (specially for the charm results).

A more detailed calculation considering the resolved part of the photon is beyond the scope of the present analysis. In Ref. [27], the resolved component is considered by including the off-shell matrix elements identical to those of heavy quark hadroproduction, convoluted with the photon and the proton unintegrated parton densities. In Ref. [37], where the color dipole picture is applied to heavy quark photoproduction using the saturation model, a vector dominance model contribution is included. In our analysis, we only consider the matrix elements of the direct component of the photon. According to the authors of Ref. [39], the $\gamma \to c\bar{c}$ component of the photon is automatically included in the $k_\perp$-factorization approach, since there is no restriction on the transverse momenta along the evolution chain. Moreover, it is shown in Ref. [39], in particular when calculating the D^* (mesons) differential cross section $d\sigma/dx_\gamma$, that part of the resolved photon contribution is effectively included by the BFKL or Ciafaloni-Catani-Fiorani-Marchesini (CCFM) [40] evolution, namely, this is included in the evolution of the unintegrated gluon distribution, and the off-shell matrix elements contain only the direct component of the photon. When using such approaches in photoproduction, the resolved photon contribution is in general not included explicitly in order to avoid double counting, since the off-shell gluon from the BFKL evolution already takes into account a certain portion of this contribution.

In order to investigate the influence of the procedures above on the predictions for the total cross section and to find the source (in the transverse momentum range) of the main contribution, we propose to consider the $k_\perp$ profile of the unintegrated cross section. This quantity, denoted by $W(x,k_\perp^2)$, is obtained by unfolding the $k_\perp^2$ integration in Eq. (11). In Fig. 4 we show the profile functions for charm obtained by using the saturation model (plot on the left) and the derivative of the collinear gluon distribution (plot on the right), for fixed target energies (momentum fraction $x = 10^{-2}$) and high energies ($x = 10^{-4}$). For the saturation model, we consider two of the procedures above, namely, the dipole approximation (fixed α_s and $x_2 = x_{Bj}$) and the semihard approach (α_s running with $\mu^2 = p_\perp^2 + m_Q^2$ and $x_2 = 2x_{Bj}$). At $x = 10^{-2}$ the profile functions are peaked around $k_\perp^2 \simeq 0.3$ GeV^2, whereas at $x = 10^{-4}$ the peaks are shifted toward $k_\perp^2 \simeq 1$ GeV^2. As expected from results for the total cross section (Fig. 3), the semihard approach results have a larger normalization than the dipole ones. An important feature emerging from these results is the dominance of the small-$k_\perp^2$ region for the charm total cross section. Indeed, at high energies the peak is of the order of the saturation scale, $k_\perp^2 \simeq Q_s^2$, and contributions for $k_\perp^2 \gtrsim 10$ GeV^2 are negligible.

For the derivative of the collinear gluon distribution (usually denoted d-gluon), we choose the scale $\mu^2 = p_\perp^2 + m_Q^2$ and $x_2 = 2x_{Bj}$. We can notice in the right panel of Fig. 4 the effect of the discontinuity in the derivative of the gluon function, Eq. (21), at $Q_0^2 = 0.8$ GeV^2: the profile function peaks at this value for $k_\perp^2 \geqslant Q_0^2$, whereas it has a flatter behavior for $k_\perp^2$ below Q_0^2. We can also notice that the $k_\perp$ profile for the derivative of the gluon distribution is broader than in the saturation model. Still the main contribution comes from the small-$k_\perp$ region; however, intermediate values of transverse momentum give a considerable contribution. This will bring the predictions closer to data, as we will see later on.

In Fig. 5 we present the results for the $k_\perp$ profile for the bottom, where we compare the different procedures and unintegrated gluon functions, as in the charm case. Some differences in comparison with the charm are evident. For the saturation model calculations, the results of the dipole and semihard procedures are very similar, since the scale μ^2

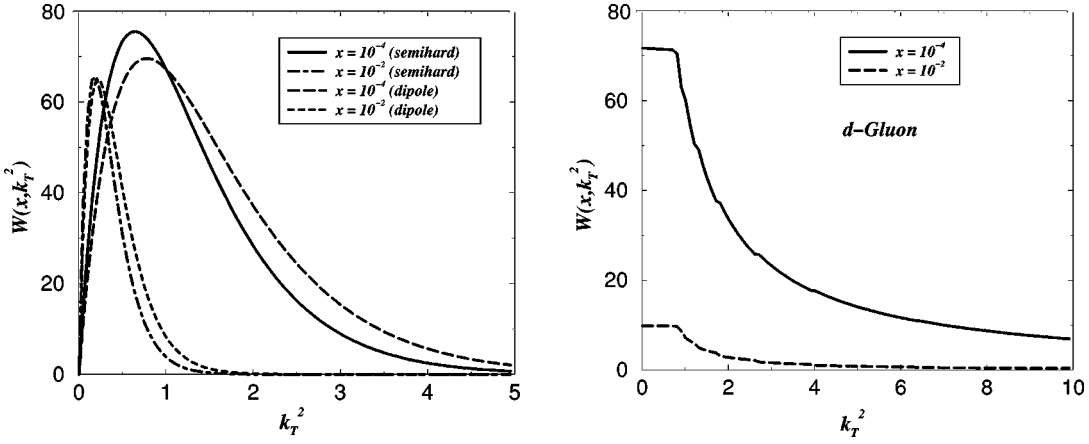

FIG. 5. Left plot: The $\boldsymbol{k}_\perp$ profile (bottom) for the unintegrated cross section from the saturation model for two different procedures concerning coupling constant and momentum fraction scale (see text). Right plot: The $\boldsymbol{k}_\perp$ profile (bottom) for the unintegrated cross section from the derivative of the collinear gluon distribution (LO GRV98 parametrization).

$=\boldsymbol{p}_\perp^2+m_Q^2$ provides a high virtuality even at very small transverse momentum due to the large mass of the bottom. This makes the strong coupling constant very close to the value $\alpha_s=0.2$ in the whole $\boldsymbol{p}_\perp$ range, as assumed in the original saturation model. The results from the derivative of the collinear gluon distribution keep the same features as in the charm case, having again a broader $\boldsymbol{k}_\perp$ profile in comparison with the saturation model.

The study of the $\boldsymbol{k}_\perp$ profile shows the dominant region in the $\boldsymbol{k}_\perp$ range and the effect of choosing distinct scales for the coupling and longitudinal momentum fractions. From the profiles discussed above, we expect that the broader $\boldsymbol{k}_\perp$ spectrum for the derivative of the collinear gluon function will enhance the overall normalization of the total cross section at high energies, improving the data description in comparison with the saturation model predictions. Motivated by this fact, we also perform a comparison at the total cross section level between the two unintegrated gluon functions, namely, the saturation approach and the derivative of the collinear gluon funtion. In both cases we make our default choice of scale $\mu^2=\boldsymbol{p}_\perp^2+m_Q^2$ and $x_2=2x_{Bj}$. This comparison is shown in Fig. 6 for both charm and bottom total cross sections. The saturation model underestimates high energy data, since the treatment of QCD evolution is not considered in the original model. Recent improvements, taking QCD evolution into account, should cure this shortcoming [31]. The derivative of the collinear gluon distribution gives a better description of high energy data, since it includes the gluon emission referred to above. As expected, it is in disagreement at lower energies, since the nonsinglet (valence) content was not included in the analysis. In addition, it was also verified that the corresponding unintegrated distribution function takes negative values in that region. For the sake of illustration, we also show the parton model results (collinear approach) for the LO process $\gamma g\to Q\overline{Q}$, where $m_c=1.3$ GeV, $m_b=4.75$ GeV, and $\mu^2=\hat{s}$ have been used. This gives a reasonable description of data given the use of lower heavy quark masses or alternatively considering higher order corrections to the LO calculation. In contrast, the semihard approach gives a reasonable description of data already at the LO level. The energy dependence is distinct in the calculations: the saturation model provides a mild energy growth, whereas in the collinear approach the growth is steeper. The collinear approach and the semihard result using the derivative of the gluon function present a similar energy behavior, with sizable deviations only at low energies near the threshold.

As a final investigation, we compute the $\boldsymbol{p}_\perp$ distribution for charm and bottom quarks using the saturation model (using the three procedures discussed earlier) and the derivative of the collinear gluon distribution, at center of mass energy $W=200$ GeV. The predictions are shown in Fig. 7. A remarkable feature is the finite and well controlled behavior at small $\boldsymbol{p}_\perp$ for both gluon functions. One can also see the usual falloff at large transverse momentum. The finiteness at zero

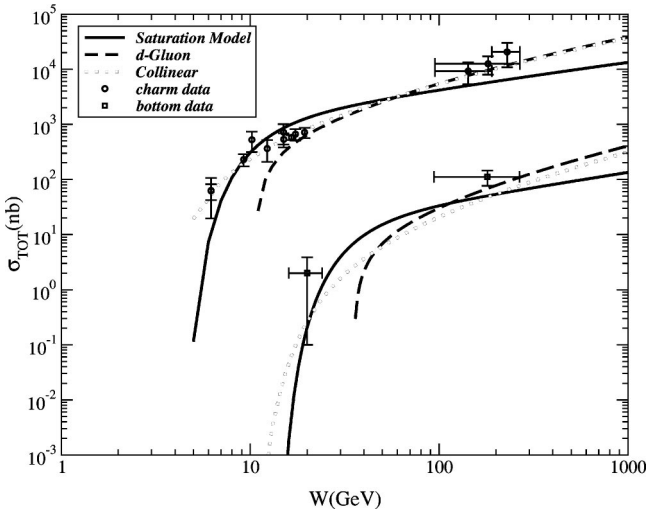

FIG. 6. The results for the charm and bottom total cross sections considering the saturation model, the derivative of the collinear gluon distribution, and the collinear parton model. See discussion in the text.

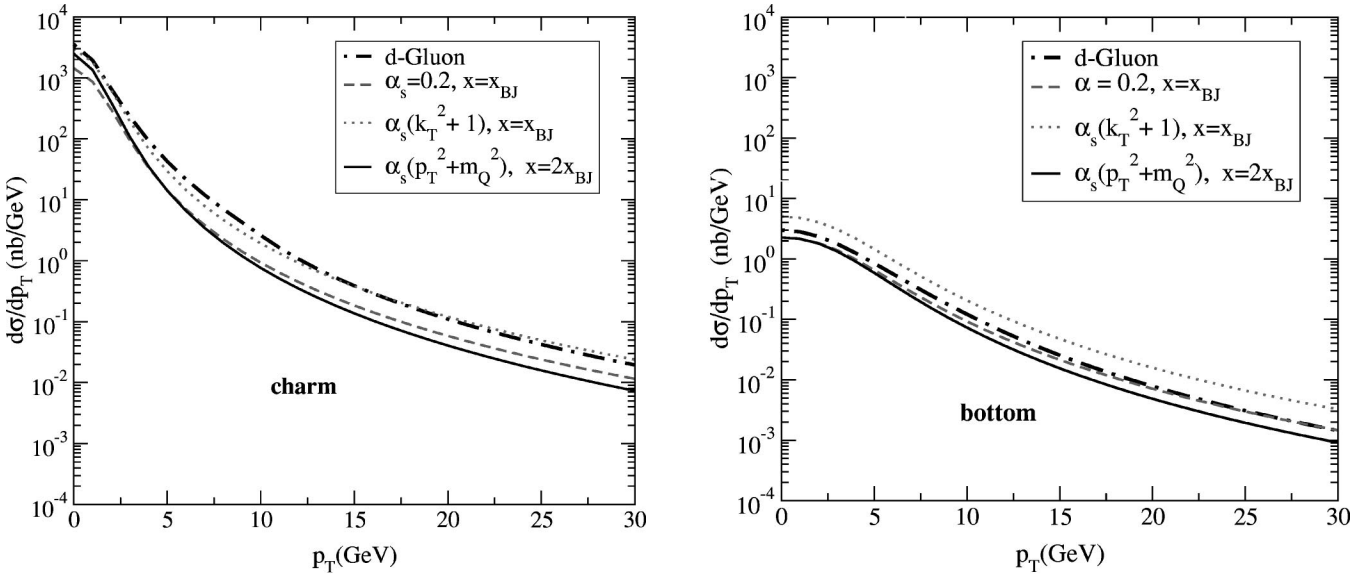

FIG. 7. Left plot: The charm $\boldsymbol{p}_\perp$-distribution from the saturation model (using three distinct procedures) and the derivative of the collinear gluon distribution for $W=200$ GeV. Right plot: The bottom $\boldsymbol{p}_\perp$ distribution from the saturation model (using three distinct procedures) and the derivative of the collinear gluon distribution for $W=200$ GeV.

transverse momentum in a LO level calculation is one of the main advantages of the semihard approach. Our results are comparable with those of Refs. [26,27], which consider other parametrizations for the unintegrated gluon function. Our results for the saturation model are quite similar, even using different prescriptions for the scales at α_s and for longitudinal momentum fraction, with a slight deviation at larger transverse momentum. The growth at small $\boldsymbol{p}_\perp$ is less steep in the bottom case than in the charm calculation, because of the larger bottom mass in the argument of α_s. The derivative of the collinear gluon distribution (d-gluon) produces a similar behavior in $\boldsymbol{p}_\perp$, but with a somewhat higher overall normalization.

IV. CONCLUSIONS

In this paper we investigate in detail the $\boldsymbol{k}_\perp$-factorization approach (semihard approach) applied to heavy quark photoproduction. In this formalism the cross section is given by the convolution of off-shell matrix elements with the unintegrated parton distributions $\mathcal{F}(x_2,\boldsymbol{k}_\perp^2)$. The matrix elements are at present known at LO accuracy, and include most of the NLO and even NNLO diagrams from the collinear factorization approach. This fact is advantageous in heavy quark production, since NLO calculations in the collinear approach undershoot data (specially Tevatron data for the bottom). There are several parametrizations for the unintegrated gluon function, relying on the solution of evolution equations or based on phenomenological considerations. We have investigated the application of the saturation model parametrization, which provide us a safe treatment of the infrared region and includes the onset of the parton saturation phenomenon. Moreover, the adjustable parameters of this model are extracted from the high energy HERA data, and therefore the results are parameter-free.

In order to go beyond the leading logarithmic approximation [$\ln(1/x)$], we let the strong coupling constant run and use a suitable longitudinal momentum fraction entering in $\mathcal{F}$. The description of the total cross section data is strongly dependent on those procedures. An additional ingredient in the calculations is a threshold correction factor accounting for the low energy behavior. The best agreement is obtained by the prescription $\mu^2=\boldsymbol{p}_\perp^2+m_Q^2$ and $x_2=2x_{Bj}$. However, in any case the saturation model slightly underestimates the high energy experimental results. This comes from the fact that QCD evolution is not present in the original model. In order to investigate the role played by these evolution emissions, we have considered the derivative of the collinear gluon distribution, which provides a closer connection with the DGLAP formalism. Indeed, the results for the charm and bottom total cross sections are in nice agreement at both low and high energies. Recent improvements of the saturation model considering these emissions are expected to produce similar results.

It was verified that the study of the $\boldsymbol{k}_\perp$ profile provides important information about the range of transverse momentum that gives the main contribution for the processes. For the saturation model the most important piece is peaked at the saturation scale $\boldsymbol{k}_\perp^2\simeq Q_s^2$. The $\boldsymbol{k}_\perp$ spectrum is broader for the derivative of the gluon distribution $\mathcal{G}(x_2,\boldsymbol{k}_\perp^2)$. The $\boldsymbol{p}_\perp$ distribution of the produced heavy quarks is also computed, showing the effects coming from different prescriptions for the scales considered. The results for the saturation model are quite similar, even using different prescriptions for the scales at α_s and for the longitudinal momentum fraction, with a slight deviation at large transverse momentum. The growth at small $\boldsymbol{p}_\perp$ is less steep in the botton case than for the charm. The derivative of the collinear gluon distribution produces a similar behavior in $\boldsymbol{p}_\perp$.

The study of heavy quark photoproduction in the frame-

work of the semihard approach improves the understanding of QCD dynamics both in the infrared and in the perturbative regions. It also sheds light on the proton structure, especially the gluon distribution. Therefore, it contributes to the understanding of the amazing interplay of soft and hard QCD phenomena.

ACKNOWLEDGMENT

This work was supported by CNPq, Brazil. M.V.T.M. is grateful to Professor Nikolai Zotov (Skobeltsyn I.N.P., Moscow State University) and Antoni Szczurek (Institute of Nuclear Physics, Cracow) for useful enlightenment.

[1] M. Klasen, hep-ph/0206169.
[2] M. Kramer, Prog. Part. Nucl. Phys. **47**, 141 (2001).
[3] M. E. Hayes and M. Kramer, J. Phys. G **25**, 1477 (1999).
[4] F. Sefkow, J. Phys. G **28**, 953 (2002).
[5] J. C. Collins, D. E. Soper, and G. Sterman, in *Perturbative Quantum Chromodynamics*, edited by A. H. Mueller (World Scientific, Singapore, 1989).
[6] V. Gribov and L. Lipatov, Sov. J. Nucl. Phys. **15**, 438 (1972); L. Lipatov, *ibid.* **20**, 94 (1975); G. Altarelli and G. Parisi, Nucl. Phys. **B126**, 298 (1977); Y. Dokshitser, Sov. Phys. JETP **46**, 641 (1977).
[7] CTEQ Collaboration, H. L. Lai *et al.*, Eur. Phys. J. C **12**, 375 (2000).
[8] A. D. Martin, R. G. Roberts, W. J. Stirling, and R. S. Thorne, Eur. Phys. J. C **23**, 73 (2002).
[9] M. Gluck, E. Reya, and A. Vogt, Eur. Phys. J. C **5**, 461 (1998).
[10] S. Frixione, M. L. Mangano, P. Nason, and G. Ridolfi, Nucl. Phys. **B412**, 225 (1994); Phys. Lett. B **348**, 633 (1995).
[11] M. G. Ryskin, A. G. Shuvaev, and Y. M. Shabelski, Yad. Fiz. **64**, 2080 (2001) [Phys. At. Nucl. **64**, 1995 (2001)].
[12] C. Brenner Mariotto, M. B. Gay Ducati, and G. Ingelman, Eur. Phys. J. C **23**, 527 (2002); J. Damet, G. Ingelman, and C. B. Mariotto, J. High Energy Phys. **09**, 014 (2002).
[13] P. Nason, S. Dawson, and R. K. Ellis, Nucl. Phys. **B303**, 607 (1988); **B327**, 49 (1989); **B335**, 260(E) (1989).
[14] CDF Collaboration, F. Abe *et al.*, Phys. Rev. Lett. **71**, 500 (1993); **71**, 2396 (1993); Phys. Rev. D **53**, 1051 (1996); **55**, 2546 (1997); D0 Collaboration, S. Abachi *et al.*, Phys. Rev. Lett. **74**, 3548 (1995); Phys. Lett. B **370**, 239 (1996); D0 Collaboration, B. Abbott *et al.*, *ibid.* **487**, 264 (2000).
[15] S. Catani, M. Ciafaloni, and F. Hautmann, Nucl. Phys. **B366**, 135 (1991).
[16] J. Collins and R. Ellis, Nucl. Phys. **B360**, 3 (1991).
[17] L. Gribov, E. Levin, and M. Ryskin, Phys. Rep. **100**, 1 (1983); E. M. Levin, M. G. Ryskin, Y. M. Shabelski, and A. G. Shuvaev, Sov. J. Nucl. Phys. **53**, 657 (1991).
[18] E. Kuraev, L. Lipatov, and V. Fadin, Sov. Phys. JETP **44**, 443 (1976); **45**, 199 (1977); Y. Balitskiĭ and L. Lipatov, Sov. J. Nucl. Phys. **28**, 822 (1978).
[19] J. Bartels, S. Gieseke, and C. F. Qiao, Phys. Rev. D **63**, 056014 (2001); J. Bartels, S. Gieseke, and A. Kyrieleis, *ibid.* **65**, 014006 (2002); S. Gieseke, hep-ph/0206190; J. Bartels, D. Colferai, S. Gieseke, and A. Kyrieleis, Phys. Rev. D **66**, 094017 (2002).
[20] A. Bialas, H. Navelet, and R. Peschanski, Nucl. Phys. **B593**, 438 (2001).
[21] J. R. Forshaw, G. Kerley, and G. Shaw, Phys. Rev. D **60**, 074012 (1999); M. McDermott, L. Frankfurt, V. Guzey, and M. Strikman, Eur. Phys. J. C **16**, 641 (2000); E. Gotsman *et al.*, J. Phys. G **27**, 2297 (2001); A. Donnachie and H. G. Dosch, Phys. Rev. D **65**, 014019 (2002); M. B. Gay Ducati and M. V. T. Machado, *ibid.* **65**, 114019 (2002); M. A. Betemps, M. B. Gay Ducati, and M. V. T. Machado, *ibid.* **66**, 014018 (2002).
[22] S. Catani and F. Hautmann, Nucl. Phys. **B427**, 475 (1994).
[23] J. R. Forshaw and P. J. Sutton, Eur. Phys. J. C **1**, 285 (1998).
[24] K. Golec-Biernat, L. Motyka, and A. M. Stasto, Phys. Rev. D **65**, 074037 (2002).
[25] K. Golec-Biernat and M. Wüsthoff, Phys. Rev. D **60**, 114023 (1999); **59**, 014017 (1999).
[26] A. V. Lipatov, V. A. Saleev, and N. P. Zotov, Mod. Phys. Lett. A **15**, 1727 (2000).
[27] Y. M. Shabelski and A. G. Shuvaev, hep-ph/0107106.
[28] S. Catani, M. Ciafaloni, and F. Hautmann, Phys. Lett. B **242**, 97 (1990).
[29] S. J. Brodsky, G. P. Lepage, and P. B. Mackenzie, Phys. Rev. D **28**, 228 (1983).
[30] Small *x* Collaboration, B. Anderson *et al.*, Eur. Phys. J. C **35**, 77 (2002).
[31] J. Bartels, K. Golec-Biernat, and H. Kowalski, Phys. Rev. D **66**, 014001 (2002).
[32] H. Jung, Phys. Rev. D **65**, 034015 (2002).
[33] M. S. Atiya *et al.*, Phys. Rev. Lett. **43**, 414 (1979); WA4 Collaboration, D. Aston *et al.*, Phys. Lett. **94B**, 113 (1980); EMC Collaboration, J. J. Aubert *et al.*, Nucl. Phys. **B213**, 31 (1983); SHFP Collaboration, K. Abe *et al.*, Phys. Rev. Lett. **51**, 156 (1983); Phys. Rev. D **33**, 1 (1986); M. I. Adamovich, Phys. Lett. B **187**, 437 (1987); Tagged Photon Spectrometer Collaboration, J. C. Anjos *et al.*, Phys. Rev. Lett. **65**, 2503 (1990).
[34] H1 Collaboration, S. Aid *et al.*, Nucl. Phys. **B472**, 32 (1996).
[35] European Muon Collaboration, J. J. Aubert *et al.*, Phys. Lett. **106B**, 419 (1981).
[36] H1 Collaboration, C. Adloff *et al.*, Phys. Lett. B **467**, 156 (1999).
[37] A. Szczurek, Eur. Phys. J. C. (to be published), hep-ph/0203050.
[38] I. P. Ivanov and N. N. Nikolaev, Phys. Rev. D **65**, 054004 (2002).
[39] S. P. Baranov, H. Jung, L. Jonsson, S. Padhi, and N. P. Zotov, Eur. Phys. J. C **24**, 425 (2002).
[40] M. Ciafaloni, Nucl. Phys. **B296**, 49 (1988); S. Catani, F. Fiorani, and G. Marchesini, Phys. Lett. B **234**, 339 (1990); Nucl. Phys. **B336**, 18 (1990); G. Marchesini, *ibid.* **B445**, 49 (1995).